ACS APPLIED MATERIALS & INTERFACES

Research Article

Cite This: ACS Appl. Mater. Interfaces XXXX, XXX, XXX−XXX

www.acsami.org

Boosting Photocatalytic Performance in Mixed-Valence MIL-53(Fe) by Changing Fe^{II}/Fe^{III} Ratio

Hui Chen,[†,§] Yutang Liu,*[,†,§] Tao Cai,[†,§] Wanyue Dong,[†,§] Lin Tang,[†,§] Xinnian Xia,[∥] Longlu Wang,[‡] and Tao Li[†,§]

[†]College of Environmental Science and Engineering and [‡]School of Physics and Electronics, Hunan University, Lushan South Road, Yuelu District, Changsha 410082, P.R. China

[§]Key Laboratory of Environmental Biology and Pollution Control (Hunan University), Ministry of Education, Lushan South Road, Yuelu District, Changsha 410082, P.R. China

[∥]College of Chemistry and Chemical Engineering, Hunan University, Changsha 410082, P.R. China

Supporting Information

ABSTRACT: One of vital issues that inhibit photoactivity of metal−organic frameworks is the poor electrical conductivity. In this work, one-dimensional mixed-valence iron chains are used to improve this poor situation in MIL-53(Fe). A series of mixed-valence MIL-53(Fe) photocatalysts were obtained through heating at different temperatures in vacuum. The effect of Fe^{II} coordinatively unsaturated metal sites (CUS) and one-dimensional mixed-valence iron chains on their photocatalytic property was discussed. The experimental results indicated that mixed-valence MIL-53(Fe) with a reference Fe^{II}/Fe^{III} ratio of 0.2725 displayed the best photocatalytic performance, which showed 96.28 and 95.01% removal efficiencies of RhB and TC-H in 100 min, respectively. Moreover, MIL-53(Fe) heated in vacuum displayed better catalytic activity than MIL-53(Fe) heated in air for RhB and TC-H degradation. Based on the analysis of various characterizations, the reinforced catalytic activity can be attributed to the charge mobilities in mixed-valence Fe^{II}/Fe^{III} chains. It is worth mentioning that the method is also applicable to MIL-88(Fe) and MIL-101(Fe). Additionally, mixed-valence MIL-53(Fe) can also perform the catalysis reaction in the nighttime by activating persulfate (PS) to produce free radicals. Interestingly, it was found that the Fe^{II} CUS lost in activating PS can be supplemented by self-reduction of photogenerated electrons during illumination in the daytime, so as to achieve a more stable cycle. This work demonstrated that the photoactivity of MIL-53(Fe) can be improved by adjusting the ratio of Fe^{II}/Fe^{III} and the feasibility of using as an all-day-active catalyst.

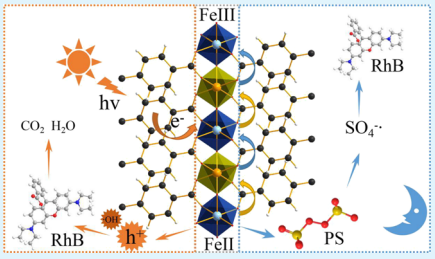

KEYWORDS: *mixed-valence MIL-53(Fe), photocatalytic degradation, persulfate, all-day-active, bifunctional catalyst*

1. INTRODUCTION

As the society and economy develop at fast pace, water environmental pollution has increasingly been a serious problem in the world. It has already been a hot research topic to explore related methods, which can efficiently remove the pollutants from a water environment because of its ecological and environmental importance.[1,2] In recent years, more and more attention has been paid to heterogeneous photocatalysis because of the widely application in environmental remediation.[2,3] It is necessary to find a high-performance, economical, and environmentally friendly photocatalyst to degrade pollutants. Metal−organic frameworks (MOFs) are crystalline porous materials, which consist of organic linkers and metal nodes.[4] Owing to the great surface areas, well-ordered porous structures, flexible organic linkers or metal nodes, and the visible light response, MOFs have attracted considerable interests to be used as a photocatalyst.[5] Many excellent materials of photocatalytic MOFs and their derivatives have been reported. The methods mainly include the following: altering metal centers or linkers[6] compounded with metal nanoparticles[7] and other functional materials (such as graphene,[8] Mxene,[9] and C3N4[10]), forming heterojunctions with other semiconductors,[11] and so on.

However, when dealing with pollutants as a photocatalyst monomer, the biggest challenge is the inefficient charge mobility of MOFs,[12] which leads to a high recombination rate of the photogenerated electrons and holes.[13] For increasing the efficiency of charge mobility in MOFs, what is worth noting is some of the MOFs have chains of the transition-metal atom bridged by an organic element, which is similar to the one-dimensional (1D) lines of inorganic semiconductors in the crystal. Charge transfer may occur preferentially in these one-dimensional wires in the crystal, which indicates a free migration of charge along the long axis of the particle.[14] Aubrey and co-workers made a particularly successful strategy for three-dimensional Fe-based conductive MOFs, increasing

Received: April 3, 2019
Accepted: July 24, 2019
Published: July 24, 2019

DOI: 10.1021/acsami.9b05829
ACS Appl. Mater. Interfaces XXXX, XXX, XXX−XXX

the conductivity by 1000 times along a single crystallographic axis.[15] In addition, a feasible strategy that engineered long-range migration through installation of mixed-valence functional sites to promote internal charge transfer was proposed.[16,17] What is more, previous studies have found that mixed-valence transition metal in photocatalysts would lead to a desirable band structure,[18] promote the transfer of photogenerated charges,[14] and increase the reactive sites,[19] and the introduction of mixed-valence transition metal for the photocatalyst is a strategy to improve photocatalytic performance.

Thus, this study chose MIL-53(Fe) as the objective photocatalyst due to the three-dimensional porous MOFs consists of infinite 1D linkage of −Fe−O−Fe−O−Fe−, which linked by a bis-bidentate terephthalate (1,4-benzenedicarboxylate) linker,[13] which could serve as a highway of charge translation.[14] What is more, MIL-53(Fe) is a photocatalyst with low cost and environmentally friendly and possess visible light response.[20,21] The preparation methods of mixed-valence MOFs have been widely reported, and the transition metal iron can be reduced by heating in vacuum. It has been proved that Fe^{II} coordinatively unsaturated metal sites (CUS) could be created through heating under a vacuum or inert atmosphere on MIL-100(Fe).[22] Meanwhile, CUS created by the removal of H_2O and other molecules (DMF or terephthalic acid) can act as an active site to modify adsorption and catalytic properties.[23] Moreover, several studies have demonstrated that heating under vacuum can create Fe^{II} CUS in MIL-53(Fe) to accelerate the activation of persulfate (PS) to degrade pollutants.[24,25] Considering another weakness of the photocatalyst that it becomes catalytically inactive when light irradiation ceases,[26] it is a valuable strategy that mixed-valence MIL-53(Fe) can be used as an all-day-active catalyst for continuously cleansing water for environmental purification by combination of photocatalysis and PS activation.[27] Also, up to the present, it is still lacking to study that mixed-valence MIL-53(Fe) was used as an independent photocatalyst to degrade contaminants and to research the effect of Fe^{II} CUS on the photocatalytic properties of MIL-53(Fe).

This exploratory study is for the feasibility of using mixed-valence MIL-53(Fe) as a photocatalyst and investigates the role of 1D mixed-valence iron chains in MIL-53(Fe). The catalytic properties of mixed-valence MIL-53(Fe) as both the photocatalyst and PS activator were investigated. Experiments have shown that mixed-valence MIL-53(Fe) could function in visible light for the degradation of rhodamine B (RhB) and tetracycline hydrochloride (TC-H) in water. The Fe^{II}/Fe^{III} reference ratio of MIL-53(Fe) is controlled within a certain range of 0−0.3983. The existence of mixed-valence Fe^{II}/Fe^{III} iron chains improves its charge mobility capacity and reduces the recombination of the electron and hole, which increasing the photocatalytic activity of MIL-53(Fe). Meanwhile, it is discovered that the performance of PS activation in the catalysts could be successfully recovered after regeneration in illumination. The results provide a simple and cheap way to improve the performance of MOFs with transition-metal cluster chains and would bring a new perspective into the design and development of highly efficient all-day-active photocatalysts.

2. EXPERIMENTAL SECTION

2.1. Chemicals. $FeCl_3·6H_2O$, 1,4-benzenedicarboxylic acid (1,4-BDC), *N*,*N*-dimethylformamide (DMF), rhodamine B (RhB), tetracycline hydrochloride (TC-H), persulfate (PS, $K_2S_2O_8$, 98.0%), and ethanol (C_2H_6O, 99.7%) were all purchased from Sinopharm Chemical Reagent Co., Ltd. The water used in this study for the preparation of all solutions was prepared by the ULUPURE purification system. All the chemical reagents were used directly without further purification.

2.2. Synthesis of a Series of Mixed-Valence MIL-53(Fe) Photocatalysts. MIL-53(Fe) was synthesized employing a solvothermal method as previously reported,[28] and a mixture of terephthalic acid (H_2BDC, 5 mmol) and ferric chloride hexahydrate ($FeCl_3·6H_2O$, 5 mmol) dissolved in *N*,*N*′-dimethylformamide (DMF, 10 mL) was transferred to a Teflon-lined pressure vessel (50 mL) and stirred for 30 min. Then, the mixture was heated at 150 °C for 3 h. Also, the suspension was filtered and washed with deionized water and ethanol. Next, the collected material was suspended in water, then stirred for 12 h to remove DMF from pores, and dried at 60 °C for 12 h to get MIL-53(Fe), named MIL-0. Finally, the powder was heated in a vacuum oven at different temperatures (120, 170, and 220 °C) for 12 h for the removal of H_2O molecules and transformation of the valence state of iron; the obtained materials were designated as MIL-vac120, MIL-vac170, and MIL-vac220. In addition, another MIL-0 was heated in air at 120 °C for 12 h, which was labeled as MIL-air120. Also, MIL-88(Fe)[29] and MIL-101(Fe)[30] were synthesized employing a solvothermal method as previously reported.

2.3. Characterization. The crystal structures and chemical composition characterization of as-prepared samples were determined by X-ray diffraction (XRD, Rigaku SmartLab) at a scanning rate of 5 min^{-1} in a 2θ range of 5−80° and X-ray photoelectron spectroscopy (XPS, Thermo Fisher Scientific, England) in which the binding energies of the MIL-53(Fe) samples were calibrated with respect to the adventitious carbon (C 1s) as a reference line at 284.8 eV. The field-emission scanning electron microscopy (FESEM, Hitachi, S-4800) and transmittance electron microscopy (TEM, JEOL, JEM-2100F) were used to observe the morphology. The UV−vis diffuse reflectance spectra (DRS) were recorded by using a UV−vis spectrophotometer (Cary 300, Varian) with the background of $BaSO_4$. The photoluminescence (PL) spectra were collected on a Hitachi F-7000 fluorescence spectrophotometer, and the excitation wavelength is 350.0 nm with a scanning speed of 240 nm/min and PMT voltage of 500 V.

2.4. Electrochemical Measurements. Electrochemical measurements were measured in 0.5 M Na_2SO_4 solution with a typical three-electrode configuration with a 300 W Xe lamp that was used as the light source. A saturated calomel electrolyte was used as a reference electrode, and a Pt coil was used as a counter electrode. The working electrode prepared by the as-prepared material thin film on fluorine-doped tin oxide (FTO) used Nafion as the adhesive. Electrochemical response was recorded with a CHI 660C electrochemical analyzer (CHI Inc., USA).

2.5. Evaluation of Catalytic Activity. Photocatalytic ability of mixed-valence MIL-53(Fe) was evaluated through the photodegradation experiment using RhB and TC-H under visible light irradiation. Typically, 4 mg of as-prepared powder was added into the reaction solution (25 mL, 20 mg/L RhB or TC-H). The suspension was stirred for 30 min under a dark environment to reach an adsorption−desorption equilibrium. After visible light illumination, which generated by a 300 W Xe lamp with a cutoff filter of 420 nm, 1 mL of suspension was taken out at a given interval time and separated through centrifugation (10000 rpm, 5 min).

All PS activation experiments were conducted in a constant room temperature at 15 °C. Similarly, the suspension of 5 mg of MIL-vac120 powder catalysts and 25 mL of RhB solution (20 mg/L) was stirred for 30 min in a dark environment to reach an adsorption−desorption equilibrium, and the degradation of RhB was initiated by rapid adding PS (10 mM) to the reaction solution. At given time intervals, 1 mL of suspension was taken out, and 1 mL of ethanol was added to the mixture to quench free radicals; after that, it was centrifuged at 10,000 rpm for 5 min. All the concentration of the reactant remained in the supernatants or filtrate was analyzed by a UV−vis spectrophotometer.

DOI: 10.1021/acsami.9b05829
ACS Appl. Mater. Interfaces XXXX, XXX, XXX−XXX

3. RESULTS AND DISCUSSION

3.1. Structural Description. The porous MIL-53(Fe) solid with a 1D pore channel system was constructed by a terephthalate anion and iron ions.[31] The morphological analysis of this mixed-valued MIL-53(Fe) was observed by scanning electron microscopy (SEM) and transmission electron microscopy (TEM). As seen from Figure 1a–g, the

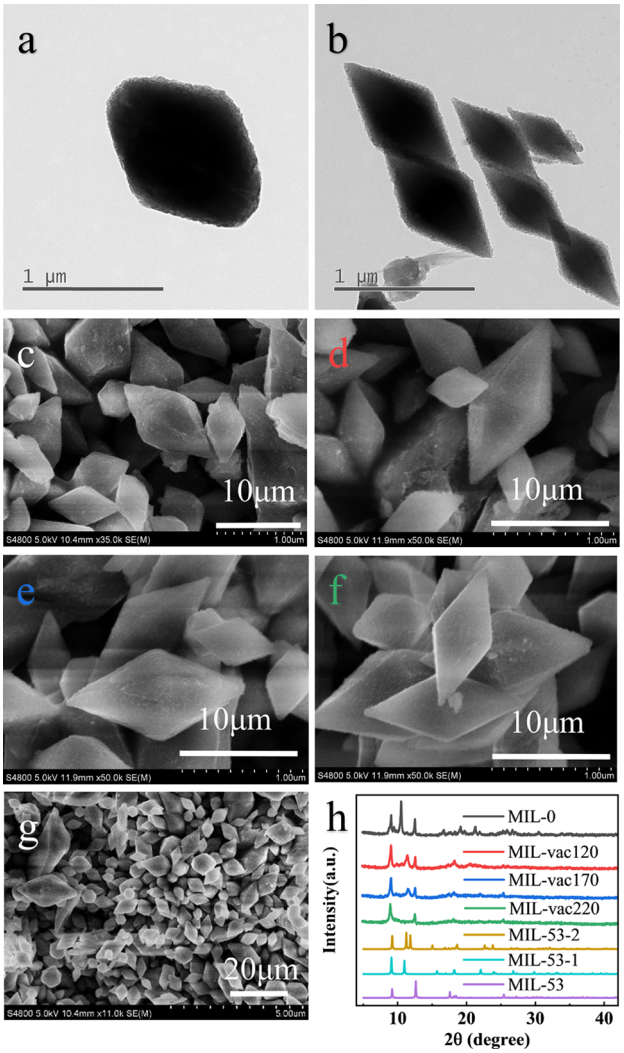

Figure 1. (a, b) TEM images of (a) MIL-0 and (b) MIL-vac120. (c–g) SEM images of (c) MIL-0, (d) MIL-vac 120, (e) MIL-vac170, and (f) MIL-vac220. (h) XRD patterns of mixed-valence MIL-53(Fe) samples and the simulated patterns of MIL-53, MIL-53-1, and MIL-53-2.

images show that the MIL-53(Fe) displayed a new cubic dodecahedral structure with a rough surface with diameters of 5–15 μm, which is similar to the MIL-53(Fe) synthesized in Changsha, Hunan Province reported in other references.[32] This is due to the different growing environment of MIL-53. Also, these samples kept intact after vacuum heating at different temperatures. This indicates that high temperature would not affect the crystal morphology. Figure 1h shows the X-ray diffraction (XRD) patterns of as-prepared samples heating under different vacuum conditions. The pattern of MIL-53(Fe) matched with the simulated MIL-53 created from CIF in ref 33 in which the characteristic peaks were at 2θ of 9.12°, 12.64°, 17.64°, 18.38°, 25.41°, and 27.27°; it was proved that MIL-53(Fe) was prepared successfully under these conditions. In addition, there are some differences in the XRD patterns of different catalysts. Therefore, two additional simulated MIL-53(Fe) XRD patterns were added to Figure 1h for comparison, one is MIL-53-1, which was bound to formic acid molecules,[34] and the other is MIL-53-2, which adsorbed a DMF molecule.[35] It can be inferred from these simulated patterns that the additional peaks between 9.12° and 25.41° were caused by the remaining DMF and its hydrolysis product inside the pores of MIL-53(Fe). With the increase of temperature, the impure peak obviously decreases or even disappears, demonstrating that the removal of DMF at high temperature. When the temperature rises, the intensities of the characteristic peaks gradually decreased, which means that heating in high temperature could destroy a partial crystal structure of MIL-53(Fe). Also, the TGA analyses of MIL-53(Fe) shown in the Supporting Information (Figure S1) prove that MIL-53(Fe) was stable enough below 340 °C.

There are two possible mechanisms for the formation of Fe^{II} CUS: the departure of anionic ligands and the reduction caused by DMF. Previous study shown in Figure 2a found that the mixed valence MIL-100(Fe) was synthesized by two-step vacuum heating treatments[22] in which the pure sample was activated under vacuum at 150 °C first, and then it was coupled with secondary vacuum between 150 and 250 °C over 12 h to get Fe^{II} CUS. The creation of Fe^{II} CUS was due to the departure of anionic ligands (F^- and OH^-) according to $Fe^{III} + X^- \rightarrow Fe^{II} + \square$ ($\square$ is the vacancy caused by the departure of anionic ligands) rather than the direct reduction of Fe^{III} CUS. Vacuum heating is also used in the production of mixed-valence MIL-53(Fe), and Fe^{II} CUS could also obtain in this way.[24] Mixed-valence MIL-53(Fe) prepared by a vacuum heating method has been reported in some previous research studies; however, the heating temperature of MIL-53(Fe) is lower than that of MIL-100(Fe).

Furthermore, the crystal structure of MIL-53(Fe)-DMF can be seen in Figure 2b, which can be considered as the structural model of MIL-0. The axial oxygen atom of terephthalate was linked by two iron octahedra, and there was a DMF molecule linked with the oxygen atom of −Fe−O−Fe− chains. In addition, Medina et al. previously discovered that the first MOF type solid of MIL-53(Fe) has a regular charge order Fe^{III}/Fe^{II} or $Fe^{III}0.5Fe^{II}0.5(OH,F)(O_2C-C_6H_4-CO_2)\cdot 0.5DMA$,[35] and the existential form of Fe^{II}/Fe^{III} in MIL-53(Fe) is a chain of alternate Fe^{II} and Fe^{III} sites. It is cause by formic acid and dimethylamine obtained by slow hydrolysis of DMF solvent, and then dimethylamine cation (DMA+) was produced according to eq 1.

$$\begin{aligned} &HCOO(CH_3)_2 + H_2O \\ &\rightarrow HCO_2H + (CH_3)_2NH \\ &\leftrightarrow HCO_2^{\cdot} + (CH_3)_2NH_2^{+} \end{aligned} \quad (1)$$

Considering about the gradually removal of DMF and water during the heating process, $Fe^{III}_xFe^{II}_{1-x}(OH)(O_2C-C_6H_4-CO_2)$ can be got by heating in vacuum. The vacuum condition would protect Fe^{II} from oxidation, and the reductibility of DMF or $HCO_2^{\cdot}$ also would result in the reduction of Fe^{III}. Meanwhile, the transformation from Fe^{II} to Fe^{III} was caused by the departure of DMF in MIL-53(Fe) when heated in air.[16] Thus, the pure MIL-53(Fe) can be acquired by heating at 120

DOI: 10.1021/acsami.9b05829
ACS Appl. Mater. Interfaces XXXX, XXX, XXX−XXX

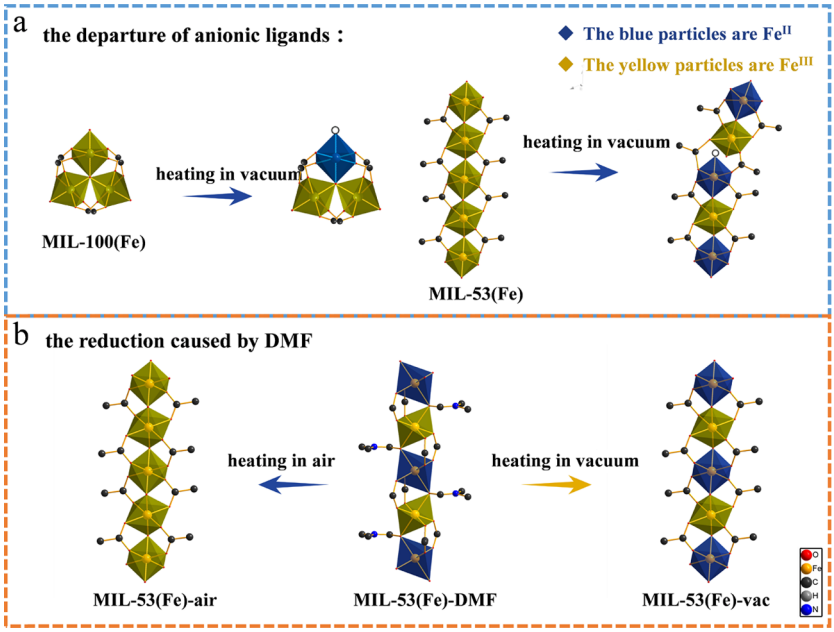

Figure 2. Material preparation process of two mechanisms for the formation of Fe^{II} CUS: (a) the departure of anionic ligands and (b) the reduction caused by DMF.

°C in air. Samples were activated in vacuum with a temperature below 220 °C for optimal integrity and efficiency of mixed-valence MIL-53(Fe). The preliminary degradation experiment shows that the photocatalytic performance of the samples heated in vacuum performed better than that of the samples heated in air. There is no doubt that the presence of Fe^{II} CUS improves photocatalytic performance.

Primarily, Figure 3a shows all the XPS spectra of Fe(2p) of the as-prepared samples. All the peaks of Fe 2p spectra shifted to the direction of lower binding energy, which proved that heating in a vacuum condition led to the reduction of Fe^{III} into Fe^{II}. Second, it was discovered from the XPS results that the MIL-0 mainly contained C, Fe, and O elements and only trace amounts of N, which means that DMF remained in the MIL-0 framework. The key role of the Fe^{II} sites was further supported by the valence of Fe composition analysis of mixed-valence MIL-53(Fe).

The XPS analysis method of iron here was borrowed from the previous report.[36] It is reported that, in the Fe(2p), the characteristic peaks at binding energies (BE) of 711.2 and 725.0 eV with a satellite signal at 719.0 eV are belonging to Fe^{III}, as well as the peaks at BE of 709.9 and 723.4 eV with a satellite signal at 715.5 eV are characteristic of Fe^{II}. Apart from the predominant Fe^{II} and Fe^{III} peaks, a higher BE energy shoulder peak was also fitted around 713.4 eV, which may be related to an interaction between Fe^{II} and Fe^{III}.[37] The ratio of the Fe^{II}/Fe^{III} XPS peak in $Fe(2p_{3/2})$ was used as a reference instead of the accurate ratio of Fe^{II}/Fe^{III} in the study. The result of XPS peak diffraction analysis is presented in Figure 3c–f. The evaluation of the surface Fe^{II}/Fe^{III} ratios from the XPS deconvolution indicated that the Fe^{II}/Fe^{III} ratio on the surface of the MIL-53(Fe) was generally increased. The calculation results are illustrated in Table 1.

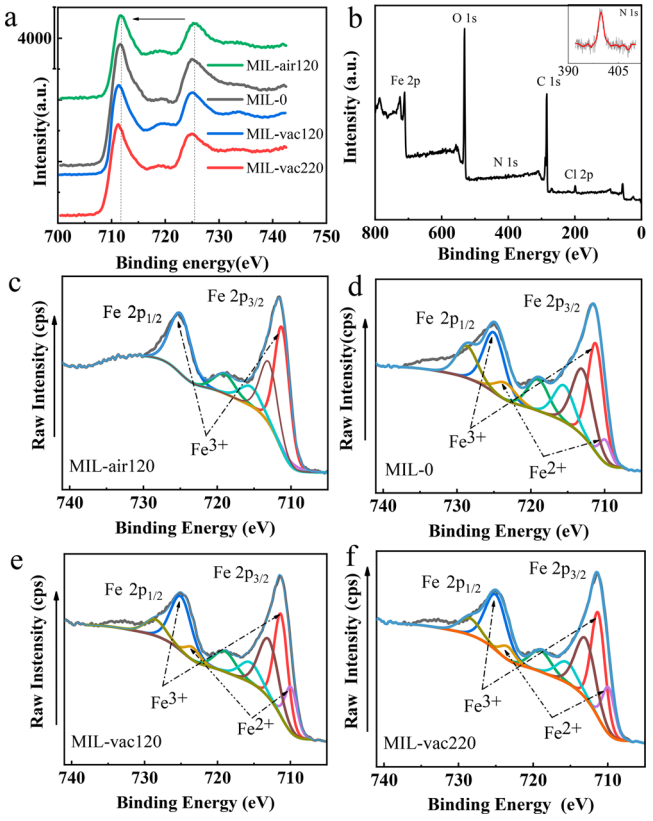

Figure 3. XPS spectra of mixed-valence MIL-53(Fe): (a) Fe 2p, (b) survey of MIL-0, and (c–f) Fe 2p of (c) MIL-air120, (d) MIL-0, (e) MIL-vac120, and (f) MIL-vac220.

3.2. Photocatalytic Reactivity. Theoretically, the presence of Fe^{II} CUS in the 1D iron chain will promote the transfer rate of the photogenerated charge and improve the efficiency of photodegradation.[16] The photoreactivity of the mixed-valence MIL-53(Fe) was evaluated by the degradation experiment of cationic dyes (RhB) and the antibiotic contaminant (TC-H) under visible light. Before illumination, the adsorption experiment toward RhB or TC-H was conducted in the dark, and the result is shown in Figure 4. Mixed-valence MIL-53(Fe) showed the absorption efficiency of RhB reached about 50% within 30 min. The good

DOI: 10.1021/acsami.9b05829
ACS Appl. Mater. Interfaces XXXX, XXX, XXX−XXX

Table 1. Reference Ratio of Fe^{II}/Fe^{III} in Mixed-Valence MIL-53(Fe)

material designation	MIL-0	MIL-vacl20	MIL-vac220	MIL-air120
ratio of Fe^{II}/Fe^{III} XPS peak in Fe($2p_{3/2}$)	0.1536	0.2725	0.3983	0

adsorption effect is due to its abundant carboxyl ligands, which attract these organic pollutants with cationic groups to close the catalytic site.[38] The photodegradation curves of RhB solution over the mixed-valence MIL-53(Fe) are shown in Figure 4a,b. Previous experiments have found that the concentration of RhB did not fluctuate significantly, which indicated that RhB was relatively stable without photocatalysts under visible light irradiation. As shown in Figure 4a, after 120 min illumination, the RhB removal efficiency in MIL-0, MIL-vac120, MIL-vac170, and MIL-vac220 reached 92.78, 96.28, 95.18, and 93.73%, respectively. With the MIL obtained at different temperatures, the effect of photodegradation gradually changes. The best photocatalytic effect can be obtained under MIL-vac120. This implies that when the reference ratio of Fe^{II}/Fe^{III} is 0.2725, the catalytic effect can be effectively improved. However, at the same time, DMF and CUS active sites induced by heating and dehydration were still present in the catalyst, which still affected photocatalytic efficiency. To eliminate the influence of DMF and CUS active sites, another sample was heated in air at the same temperature, and then their photoreactivity performance was compared. The result is shown in Figure 4b. Compared with samples heated in air, the RhB removal rate reached 84.83% in MIL-air120. To quantify the photocatalytic activity and further understand the photocatalytic kinetics for mixed-valence MIL-53(Fe), the apparent rate constant (k) of pollutant degradation was calculated with the pseudo-first-order approximation equation: $\ln(C_0/C) = kt$ in which C is the residual concentration of the pollutants at time t and C_0 is the initial concentration of the RhB or TC-H solution. The calculated results are plotted in Figure 4d,e. Therefore, the apparent rate constants of the MIL-0, MIL-vac120, MIL-air120, MIL-vac170, and MIL-vac220 are calculated to be 0.01948, 0.02993, 0.01833, 0.02509, and 0.02184 min^{-1}, respectively. The photodegradation curves toward RhB of MIL-air120 are lower than those of the samples heated in vacuum, which indicated that the presence of Fe^{II} can improve the effect of catalyst without the influence of DMF and CUS active sites.

To avoid the interference of the photocatalyst sensitized by the dye (RhB), the photocatalytic properties of the mixed-valence MIL-53(Fe) for tetracycline hydrochloride (TC-H) photodegradation were supplemented in visible light irradiation. The photolysis experiments of tetracycline hydrochloride (TC-H) proved that TC-H is very stable, which its photolysis in visible light is ignorable. Only after the addition of the photocatalyst, the concentration of TC-H in aqueous solution gradually decreased. The TC-H removal rate reached 95.01 and 71.66% in MIL-vac120 and MIL-air120, respectively (Figure 4c). Similarly, the MIL-vac120 displayed the best photocatalytic effect compared to MIL-air120, implying that the improved charge separation efficiency further enhances photocatalytic activity. In addition, the apparent reaction rate constants (k) of MIL-vac120 and MIL-air120 were about 0.02242 and 0.00917 min^{-1}, respectively (Figure 4f). Particularly, the kinetic constant of MIL-vac120 was about 2.45 times higher than that of MIL-air120.

The experiments of two Fe-based MOFs, MIL-88[39] and MIL-101,[40] have been supplemented to research a general rule in mixed-valence FeMOFs, and X-ray diffraction matched well with the corresponding simulated MIL MOFs (Figure S2, Supporting Information). It was found that these kinds of MOFs with iron metal nodes and terephthalate ligands do have universality, which the samples heated at 120 °C in vacuum showed better efficiency of photodegradation than those heated in air as shown in Figure 5. In MIL-88(Fe), The TC-H removal rate reached 64.48 and 55.84% in MIL-88-vac and MIL-88-air after 75 min, respectively (Figure 5a). In addition, the apparent reaction rate constants (k) of MIL-88-vac and MIL-88-air were about 0.01024 and 0.0069 min^{-1}, respectively (Figure 5c). Particularly, the kinetic constant of MIL-88vac was about 1.48 times higher than that of MIL-88-air. Similarly, the MIL-101vac displayed the best photocatalytic effect compared to the MIL-101-air, which showed that the TC-H

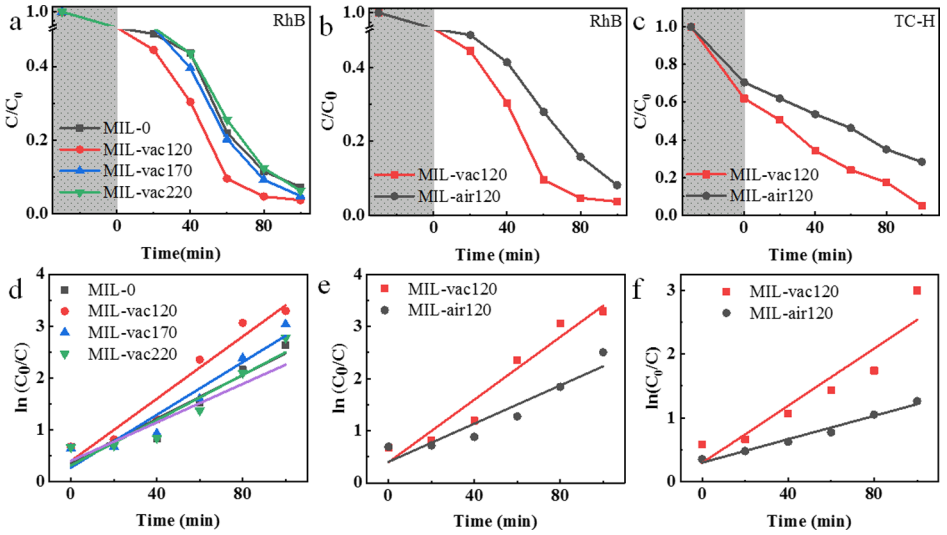

Figure 4. (a, b) Photodegradation of RhB with mixed-valence MIL-53(Fe) in visible light irradiation. (c) Photodegradation of TC-H with mixed-valence MIL-53(Fe) in visible light irradiation. (d–f) The corresponding photodegradation kinetics of RhB and TC-H with mixed-valence MIL-53(Fe) in visible light irradiation.

DOI: 10.1021/acsami.9b05829
ACS Appl. Mater. Interfaces XXXX, XXX, XXX−XXX

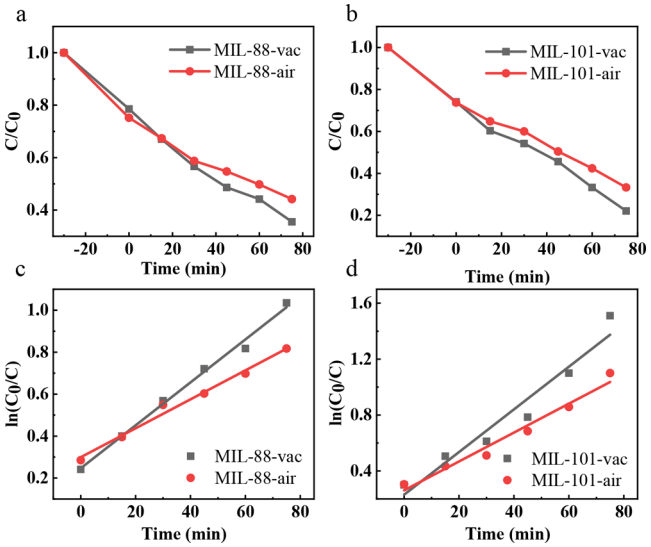

Figure 5. (a, b) Photodegradation of TC-H with mixed-valence MIL-88 and MIL-101 in visible light irradiation. (c, d) The corresponding photodegradation kinetics of TC-H with mixed-valence MIL-88 and MIL-101 in visible light irradiation.

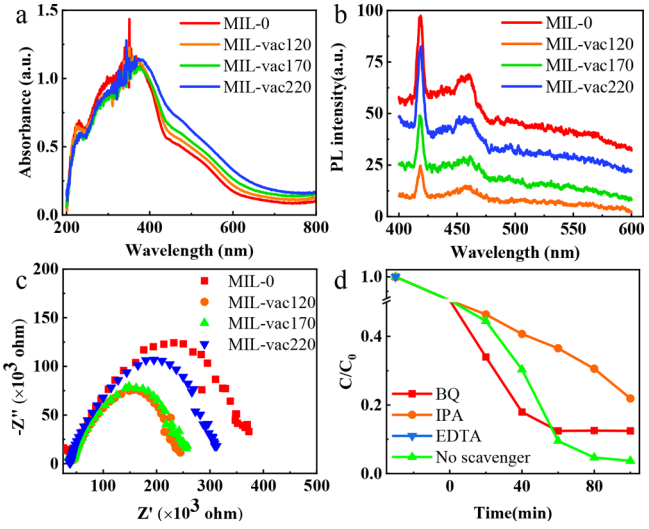

Figure 6. (a) UV−vis absorption spectra; (b) PL spectra (excitation wavelength: 350 nm); (c) EIS Nyquist plots (0.5 M Na_2SO_4 solution under dark condition) of mixed-valence MIL-53(Fe); (d) photodegradation of RhB over mixed-valence MIL-53(Fe) in the presence of trapping systems.

removal rates of MIL-101-vac and MIL-101-air reached 77.92 and 66.72% after 100 min, respectively (Figure 5b). Also, the apparent reaction rate constants (k) were about 0.01526 and 0.01033 min^{-1} in MIL-101-vac and MIL-101-air, respectively (Figure 5d). It implies that the improved charge separation efficiency of iron clusters also enhances photocatalytic activity, similarly.

3.3. Mechanism of Degradation. According to the above experimental results, it can be concluded that the change of the photocatalytic activity of mixed-valence MIL-53(Fe) was in accordance with some regularity in the relative content ratio of Fe^{II}/Fe^{III}. To understand the regulated changes of photo-excited mixed-valence MIL-53(Fe) photocatalysts, the optical properties of as-prepared samples were investigated by UV−vis diffuse reflectance spectroscopy (DRS). The UV−vis absorption spectra is shown in Figure 6a, which indicated the effect of Fe^{II} on light absorption. As can be seen from the figure, all MIL-53(Fe) samples exhibited excellent absorption in a region of 200−600 nm, which were keeping with the ligand-to-metal charge transfer (LMCT) and n−π and π−π transitions within the ligand,[41,42] and the curve shows gradually redshift by altering the Fe^{II}/Fe^{III} ratio. As shown in the inset in Figure S3, the band gap (E_g) of mixed-valence MIL-53(Fe) was evaluated from a plot of the Kubelka−Munk method from which the E_g's of MIL-0, MIL-vac120, MIL-vac170, and MIL-vac220 were calculated to be 2.76, 2.70, 2.64, and 2.58 eV, respectively. To further understand the source of light harvesting ability, the band structures of as-prepared samples were examined by the Mott−Schottky measurement, which is a tool to determine the flat band potential (E_{fb}). As depicted in Figure S4, the flat band potential of mixed-valence MIL-53(Fe) was measured by extrapolation of the Mott−Schottky plot in 0.1 M Na_2SO_4 solution at 1500 kHz. It was estimated as approximately −0.47, −0.43, −0.36, and − 0.30 V versus SCE at pH 7, corresponding to −0.23, −0.19, −0.12, and −0.06 V versus the normal hydrogen electrode (NHE). In addition, the positive linear slope of $1/C^2$ versus the potential curve indicates that MIL-53(Fe) is an n-type semiconductor. The conduction band potential (E_{cb}) is usually approximate to the conduction band of n-type semiconductors ($E_{cb} \approx E_{fb}$, −0.1 V).[43] As a result, the E_{cb} of the mixed-valence MIL-53(Fe) is approximately −0.33, −0.29, −0.22, and −0.16 V versus NHE. According to the experience formula, the valence band potential (E_{vb}) can be calculated from a formula of $E_{vb} = E_g + E_{cb}$. Correspondingly, the calculation results of valence band potential (E_{vb}) are 2.43, 2.41, 2.42, and 2.42 V. The results are also shown in Figure 7. Meanwhile, the color of catalysts

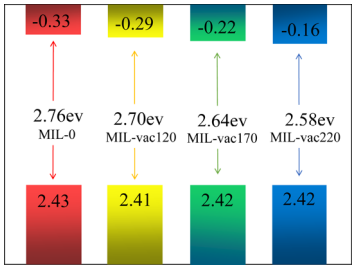

Figure 7. Band gap structure of mixed-valence MIL-53(Fe).

gradually deepened from pale yellow to dark yellow (Figure S5, Supporting Information); the change of the band structure and color correlated with the ratio of Fe^{II}/Fe^{III}, which was ascribed to Fe^{2+}−Fe^{3+} intervalence charge transfer in iron oxoclusters.[44]

Afterward, the charge transfer process was studied by PL spectroscopy and EIS. As shown in Figure 6b,c, with increasing temperature, the intension of PL emissions and EIS Nyquist plots showed a regular trend. The intension of PL emissions gradually decreased and then began to increase, and the minimum fluorescence radiation intensity appears on MIL-vac120. Similarly, compared with other samples, the arc radius of EIS Nyquist plots of MIL-vac120 is the smallest, and it is proved that MIL-vac120 has the minimum impedance on a macrolevel, which demonstrated a more effective separation of carriers. Above all, Fe^{II} CUS does facilitate the charge translation within MIL-53(Fe).

To have a clear understanding of the degradation process, it is significant to define active oxidant species participated in the

DOI: 10.1021/acsami.9b05829
ACS Appl. Mater. Interfaces XXXX, XXX, XXX−XXX

degradation process, such as superoxide radicals ($^{\cdot}O_2^-$), h^+, and hydroxyl radicals ($^{\cdot}OH$); these are generally considered as the main active oxidant, which may degrade organics.[28] Therefore, in the photocatalytic degradation process, the study chose RhB as target organics to estimate the role of these active substances in the presence of corresponding scavengers. Benzoquinone (BQ), isopropanol (IPA), and ethylene diamine tetraacetic acid disodium salt (EDTA) were employed as scavenging agents to eliminate $^{\cdot}O_2^-$, $^{\cdot}OH$, and h^+, respectively.[45] Figure 6d shows the photodegradation curve of RhB in the presence of different scavenging agents. As shown in the figure, the addition of EDTA largely inhibited the photodegradation reaction, and the presence of IPA also showed a partial inhibition effect, while the addition of BQ had no effect in the first hour of the photodegradation of RhB, but it becomes an inhibitory effect at last. Detailed data of quantitative analysis are as follows that the RhB removal efficiency decreased 15.76, 37.56, and 99.94% with addition of BQ, IPA and EDTA, respectively. The addition of EDTA and TBA can induce an obvious decrease in photocatalytic activity of MIL-vac120, while the BQ has a promoting effect on the initial photodegradation of RhB, but it becomes an inhibitory effect at last. This means that photogenerated electrons in the CB of MIL-vac120 (−0.29 V vs NHE at pH = 7) can reduce O_2 into $^{\cdot}O_2^-$ (−0.28 V vs NHE, pH = 7),[46] and partial photogenerated holes in the VB of MIL-vac120 (+2.41 V vs NHE at pH = 7) can oxidize H_2O into $^{\cdot}OH$ (+2.27 V vs NHE, pH = 7).[46] It proves that light-induced holes are the main radicals in the photodegradation of organic compounds, and the $^{\cdot}OH$ and $^{\cdot}O_2^-$ have been at least partly responsible for RhB photodegradation. In the initial photodegradation of RhB, photogenerated electrons are consumed with BQ, and the hole oxidation process is promoted.

3.4. Stability Test and All-Day Activity. The stability of MOFs is always a dilemma before putting into practical applications,[47] so it is important to investigate the stability of mixed-valence MIL-53 under visible light. Our study also evaluated the stability of MIL-vac120 through testing the RhB degradation repeatedly for five times. The degradation curve is shown in Figure S6. In five cycles, the effect of MIL-vac120 became weak gradually, the RhB removal rate after 120 min ranged from 99.45 to 69.48%, and this is because of the iron node of MIL-vac120 that was oxidized into Fe^{III} or iron oxide by photogenerated holes under long light irradiation. It is also shown by the XPS spectrum (Figure 8a) that the Fe^{II} peak (Fe 2p3/2) decreased significantly after the photodegradation reaction. The problem of photocorrosion can be solved by forming heterojunction with other functional materials to donate the extra holes.[48,49]

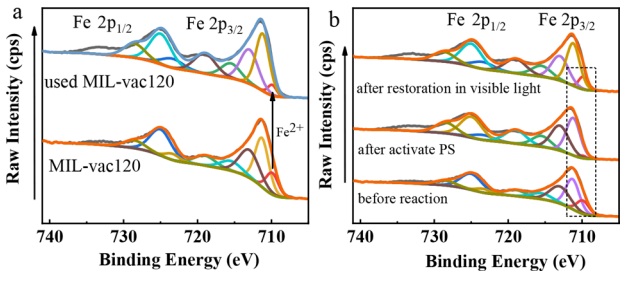

Figure 8. XPS spectra (Fe 2p) of (a) MIL-vac120 and used MIL-vac120 and (b) the changes of iron valences in MIL-vac120 during the reaction of activating PS.

In photocatalytic applications, another vital issue is that the photocatalyst may become catalytically inactive when light irradiation ceases, which means light illumination is the requisite of the photocatalyst to perform redox reactions.[50] In the dark, charge carrier generation within MIL-vac120 is suspended. However, MIL-53(Fe) has been confirmed to have properties of activated peroxides such as PS[27] and H_2O_2[51] due to the existence of Fe^{II} and Fe^{III}. The ability to maintain the catalytic activity in a dark environment has thus been the ultimate goal for photocatalysts.[52] Thus, mixed-valence MIL-53(Fe) can couple photocatalysis and the persulfate catalyst to keep degradation efficiency in day and night. Mixed-valence MIL-53(Fe) has a good efficiency to activate PS, and the presence of Fe^{II} CUS greatly enhances the catalytic activity of MIL-53(Fe).[53] The dissolved iron and the loss of Fe^{II} CUSs were unavoidable in a long heterogeneous Fenton process, observably, as shown in Figure 9c. After five cycles, the degradation of RhB decreased from 99.48 to 31.75% (each cycle is 12 h, which simulated the whole night). In the article reported by Tang and Wang, Fe^{II} CUS can be reactivated to reduce partial catalytic activities under vacuum conditions,[53] but recycling of powder catalysts is difficult to achieve in the large-scale water. MIL-53(Fe), however, is a photocatalyst, which can generate electrons by illumination to reduce Fe^{III} into Fe^{II}. As shown in Figure 9a,b, the weakened effect can be relieved through giving 30 min of illumination before each cycle reacted with PS. The degradation rate of the RhB could be maintained at a relative stable level of 45.7% after five cycles, as shown in Figure 9b. As shown in Figure 8b, the revivification of Fe^{II} CUS from illumination can also be confirmed by the XPS spectra of the sample before and after the reaction. It can be clearly observed from Figure 8b that the Fe^{II} peak disappears basically after activation of PS, while the Fe^{II} peak reappears partly after illumination, which means that most Fe^{III} was reduced to Fe^{II}. This proves that illumination in daylight can be useful to MIL-vac120 to maintain catalytic activity. The experimental result provided proof that MIL-vac120 has the potential of all-day-active catalytic degradation in environment purification.

4. CONCLUSIONS

To sum up, it is the first time to discover that MIL-53(Fe) can improve its photocatalytic performance by changing the ratio of Fe^{II}/Fe^{III}. The XPS showed that the increased ratio of Fe could indeed be obtained by vacuum heating in different temperatures. The increase of the ratio in the light absorption of MIL-53(Fe) was improved to a visible light region, and the band gap gradually decreases from 2.76 to 2.58 eV. However, with the result showed in XRD and PL, the gradually decreasing crystal peak and the increasing fluorescence indicate that the structure of 1D iron chains in MIL-53(Fe) will be broken by high temperature because of the disappearance of the ligand in iron oxide octahedron. Thus, the degradation rate of MIL-vac220 is lower than the others. The best effective photocatalyst in this experiment is MIL-vac120 with about RhB and TC-H degradation rates of 96.28 and 95.01% at 100 min, respectively; its reference ratio of Fe^{II}/Fe^{III} is 0.2725 prepared by heating at 120 °C in a vacuum condition and also presents minimal fluorescence and minimal electrochemical impedance, which were due to the addition of Fe^{II} that can translate a photogenerated charge through an exchanging

DOI: 10.1021/acsami.9b05829
ACS Appl. Mater. Interfaces XXXX, XXX, XXX−XXX

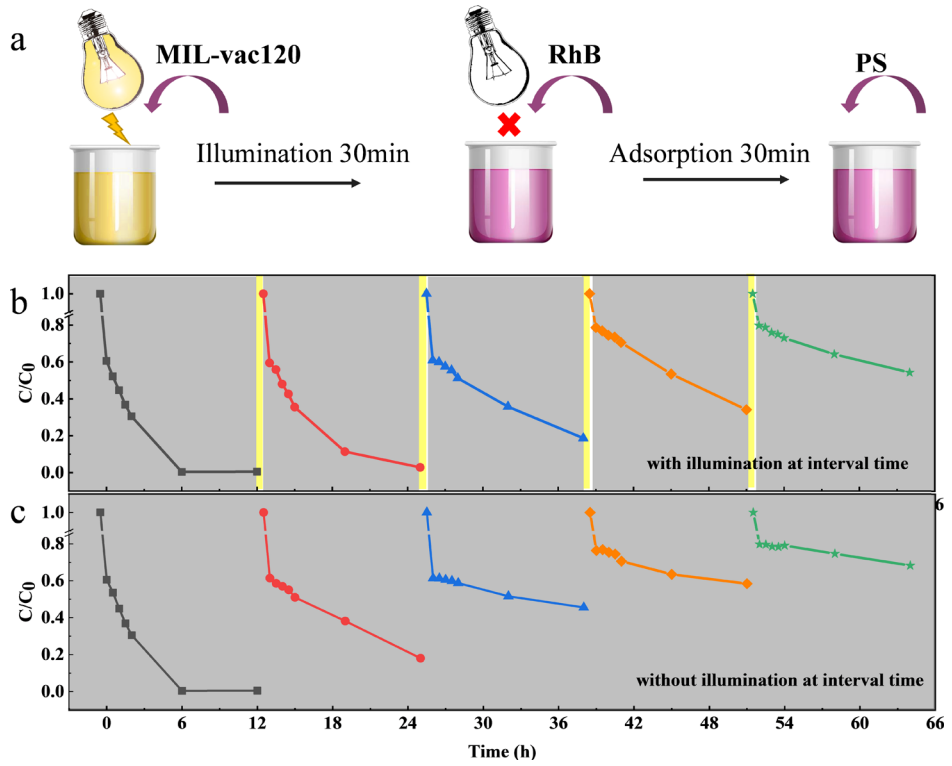

Figure 9. (a) Simulation all-day experimental flow chart. (b) Degradation of RhB used as the PS activator after illumination. (c) Degradation of RhB used as the PS activator without illumination.

valence state in 1D iron chains. Besides, as Fe-based MOFs, MIL-53(Fe) can effectively active PS into $^{\cdot}SO_4^-$. Thus, MIL-53(Fe) can be used as an uninterrupted catalyst to degrade pollutants on dark nights or cloudy days. Fe CUS is also an active site that rapidly activates PS to degrade pollutants in the time of one night under low PS concentration. During a light–dark cycle, the Fe^{II} CUS expended at night would be replenished by absorbing light to reduce itself. We believe that mixed-valence MIL-53(Fe) would perform great potential in all-day photocatalytic wastewater treatment.

■ ASSOCIATED CONTENT

Supporting Information

The Supporting Information is available free of charge on the ACS Publications website at DOI: 10.1021/acsami.9b05829.

Analysis method and characterization of the samples (PDF)

(PDF)

■ AUTHOR INFORMATION

Corresponding Author

*E-mail: yt_liu@hnu.edu.cn.

ORCID

Yutang Liu: 0000-0002-4975-364X

Notes

The authors declare no competing financial interest.

■ ACKNOWLEDGMENTS

This work was supported by the National Natural Science Foundation of China (51872089, 51478171 and 51672077), Hunan Provincial Natural Science Foundation of China (2017JJ2026), and Jiangxi Provincial Open Foundation of China (ES201880051).

■ REFERENCES

(1) Zou, J.-P.; Chen, Y.; Liu, S.-S.; Xing, Q.-J.; Dong, W.-H.; Luo, X.-B.; Dai, W.-L.; Xiao, X.; Luo, J.-M.; Crittenden, J. Electrochemical Oxidation and Advanced Oxidation Processes Using a 3D Hexagonal Co3O4 Array Anode for 4-Nitrophenol Decomposition Coupled with Simultaneous CO2 Conversion to Liquid Fuels via a Flower-Like Cuo Cathode. *Water Res.* **2019**, *150*, 330–339.

(2) Zhou, G.; Wu, M.-F.; Xing, Q.-J.; Li, F.; Liu, H.; Luo, X.-B.; Zou, J.-P.; Luo, J.-M.; Zhang, A.-Q. Synthesis and Characterizations of Metal-Free Semiconductor/Mofs with Good Stability and High Photocatalytic Activity for H2 Evolution: A Novel Z-Scheme Heterostructured Photocatalyst Formed by Covalent Bonds. *Appl. Catal., B* **2018**, *220*, 607–614.

(3) Li, F.; Wang, D.; Xing, Q.-J.; Zhou, G.; Liu, S.-S.; Li, Y.; Zheng, L.-L.; Ye, P.; Zou, J.-P. Design and Syntheses of MOF/COF Hybrid Materials via Postsynthetic Covalent Modification: An Efficient Strategy to Boost the Visible-Light-Driven Photocatalytic Performance. *Appl. Catal., B* **2019**, *243*, 621–628.

(4) Qiu, J.; Zhang, X.; Feng, Y.; Zhang, X.; Wang, H.; Yao, J. Modified Metal-Organic Frameworks as Photocatalysts. *Appl. Catal., B* **2018**, *231*, 317–342.

(5) Wang, C.-C.; Li, J.-R.; Lv, X.-L.; Zhang, Y.-Q.; Guo, G. Photocatalytic Organic Pollutants Degradation in Metal–Organic Frameworks. *Energy Environ. Sci.* **2014**, *7*, 2831–2867.

(6) Kim, M.; Cahill, J. F.; Fei, H.; Prather, K. A.; Cohen, S. M. Postsynthetic Ligand and Cation Exchange in Robust Metal-Organic Frameworks. *J. Am. Chem. Soc.* **2012**, *134*, 18082–18088.

(7) Choi, K. M.; Kim, D.; Rungtaweevoranit, B.; Trickett, C. A.; Barmanbek, J. T. D.; Alshammari, A. S.; Yang, P.; Yaghi, O. M. Plasmon-Enhanced Photocatalytic CO_2 Conversion within Metal–Organic Frameworks under Visible Light. *J. Am. Chem. Soc.* **2017**, *139*, 356–362.

DOI: 10.1021/acsami.9b05829
ACS Appl. Mater. Interfaces XXXX, XXX, XXX–XXX

(8) Lin, R.; Shen, L.; Ren, Z.; Wu, W.; Tan, Y.; Fu, H.; Zhang, J.; Wu, L.; et al. *Chem. Commun.* **2014**, *50*, 8533−8535.
(9) Tian, P.; He, X.; Zhao, L.; Li, W.; Fang, W.; Chen, H.; Zhang, F.; Huang, Z.; Wang, H. Enhanced Charge Transfer for Efficient Photocatalytic H2 Evolution over UiO-66-NH_2 with Annealed Ti_3C_2Tx Mxenes. *Int. J. Hydrogen Energy* **2019**, *44*, 788−800.
(10) Wang, C.-C.; Yi, X.-H.; Wang, P. Powerful Combination of Mofs and C3N4 for Enhanced Photocatalytic Performance. *Appl. Catal., B* **2019**, *247*, 24−48.
(11) Wang, C.-C.; Du, X.-D.; Li, J.; Guo, X.-X.; Wang, P.; Zhang, J. Photocatalytic Cr(VI) Reduction in Metal-Organic Frameworks: A Mini-Review. *Appl. Catal., B* **2016**, *193*, 198−216.
(12) Nasalevich, M. A.; van der Veen, M.; Kapteijn, F.; Gascon, J. Metal−Organic Frameworks as Heterogeneous Photocatalysts: Advantages and Challenges. *CrystEngComm* **2014**, *16*, 4919−4926.
(13) Wang, W.; Xu, X.; Zhou, W.; Shao, Z. Recent Progress in Metal-Organic Frameworks for Applications in Electrocatalytic and Photocatalytic Water Splitting. *Adv. Sci.* **2017**, *4*, 1600371.
(14) Dhakshinamoorthy, A.; Asiri, A. M.; García, H. Metal-Organic Framework (MOF) Compounds: Photocatalysts for Redox Reactions and Solar Fuel Production. *Angew. Chem. Int. Ed. Engl.* **2016**, *55*, 5414−5445.
(15) Aubrey, M. L.; Wiers, B. M.; Andrews, S. C.; Sakurai, T.; Reyes-Lillo, S. E.; Hamed, S. M.; Yu, C.-J.; Darago, L. E.; Mason, J. A.; Baeg, J.-O.; Grandjean, F.; Long, G. J.; Seki, S.; Neaton, J. B.; Yang, P.; Long, J. R. Electron Delocalization and Charge Mobility as a Function of Reduction in a Metal−Organic Framework. *Nat. Mater.* **2018**, *17*, 625−632.
(16) Combelles, C.; Ben Yahia, M.; Pedesseau, L.; Doublet, M. L. FeII/FeIII Mixed-Valence State Induced by Li-Insertion into the Metal-Organic-Framework MIL53(Fe): A DFT+U Study. *J. Power Sources* **2011**, *196*, 3426−3432.
(17) Darago, L. E.; Aubrey, M. L.; Yu, C. J.; Gonzalez, M. I.; Long, J. R. Electronic Conductivity, Ferrimagnetic Ordering, and Reductive Insertion Mediated by Organic Mixed-Valence in a Ferric Semiquinoid Metal-Organic Framework. *J. Am. Chem. Soc.* **2015**, *137*, 15703−15711.
(18) Manikandan, M.; Tanabe, T.; Li, P.; Ueda, S.; Ramesh, G. V.; Kodiyath, R.; Wang, J.; Hara, T.; Dakshanamoorthy, A.; Ishihara, S.; Ariga, K.; Ye, J.; Umezawa, N.; Abe, H. Photocatalytic Water Splitting under Visible Light by Mixed-Valence Sn3O4. *ACS Appl. Mater. Interfaces* **2014**, *6*, 3790−3793.
(19) Sahoo, D. P.; Patnaik, S.; Rath, D.; Nanda, B.; Parida, K. Cu@CuO Promoted g-C3N4/MCM-41: An Efficient Photocatalyst with Tunable Valence Transition for Visible Light Induced Hydrogen Generation. *RSC Adv.* **2016**, *6*, 112602−112613.
(20) Zhang, C.; Ai, L.; Jiang, J. Solvothermal Synthesis of MIL−53(Fe) Hybrid Magnetic Composites for Photoelectrochemical Water Oxidation and Organic Pollutant Photodegradation under Visible Light. *J. Mater. Chem. A* **2015**, *3*, 3074−3081.
(21) Laurier, K. G. M.; Vermoortele, F.; Ameloot, R.; De Vos, D. E.; Hofkens, J.; Roeffaers, M. B. J. Iron(III)-Based Metal-Organic Frameworks as Visible Light Photocatalysts. *J. Am. Chem. Soc.* **2013**, *135*, 14488−14491.
(22) Yoon, J. W.; Seo, Y.-K.; Hwang, Y. K.; Chang, J.-S.; Leclerc, H.; Wuttke, S.; Bazin, P.; Vimont, A.; Daturi, M.; Bloch, E.; Llewel lyn, P. L.; Serre, C.; Horcajada, P.; Grenèche, J. M.; Rodrigues, A. E.; Férey, G. Controlled Reducibility of a Metal-Organic Framework with Coordinatively Unsaturated Sites for Preferential Gas Sorption. *Angew. Chem. Int. Ed.* **2010**, *49*, 5949−5952.
(23) Wang, D.; Huang, R.; Liu, W.; Sun, D.; Li, Z. Fe-Based MOFs for Photocatalytic CO_2 Reduction: Role of Coordination Unsaturated Sites and Dual Excitation Pathways. *ACS Catal.* **2014**, *4*, 4254−4260.
(24) Pu, M.; Ma, Y.; Wan, J.; Wang, Y.; Wang, J.; Brusseau, M. L. Activation Performance and Mechanism of a Novel Heterogeneous Persulfate Catalyst: metal−organic Framework MIL-53(Fe) with FeII/FeIIImixed-valence coordinatively Unsaturated Iron Center. *Catal. Sci. Technol.* **2017**, *7*, 1129−1140.
(25) Wang, M.; Yang, L.; Guo, C.; Liu, X.; He, L.; Song, Y.; Zhang, Q.; Qu, X.; Zhang, H.; Zhang, Z.; Fang, S. Bimetallic Fe/Ti-Based Metal-Organic Framework for Persulfate-Assisted Visible Light Photocatalytic Degradation of Orange II. *ChemistrySelect* **2018**, *3*, 3664−3674.
(26) Cai, T.; Liu, Y.; Wang, L.; Zhang, S.; Ma, J.; Dong, W.; Zeng, Y.; Yuan, J.; Liu, C.; Luo, S. ″Dark Deposition″ of Ag Nanoparticles on TiO2: Improvement of Electron Storage Capacity to Boost ″Memory Catalysis″ Activity. *ACS Appl. Mater. Interfaces* **2018**, *10*, 25350−25359.
(27) Li, R.; Chen, Z.; Cai, M.; Huang, J.; Chen, P.; Liu, G.; Lv, W. Improvement of Sulfamethazine Photodegradation by Fe(III) Assisted MIL-53(Fe)/Percarbonate System. *Appl. Surf. Sci.* **2018**, *457*, 726−734.
(28) Liu, Q.; Zeng, C.; Ai, L.; Hao, Z.; Jiang, J. Boosting Visible Light Photoreactivity of Photoactive Metal-Organic Framework: Designed Plasmonic Z-Scheme Ag/AgCl@MIL-53-Fe. *Appl. Catal., B* **2018**, *224*, 38−45.
(29) Xie, D.; Ma, Y.; Gu, Y.; Zhou, H.; Zhang, H.; Wang, G.; Zhang, Y.; Zhao, H. Bifunctional NH2-MIL-88(Fe) Metal−Organic Framework Nanooctahedra for Highly Sensitive Detection and Efficient Removal of Arsenate in Aqueous Media. *J. Mater. Chem. A* **2017**, *5*, 23794−23804.
(30) Wang, D.; Jia, F.; Wang, H.; Chen, F.; Fang, Y.; Dong, W.; Zeng, G.; Li, X.; Yang, Q.; Yuan, X. Simultaneously Efficient Adsorption and Photocatalytic Degradation of Tetracycline by Fe-Based MOFs. *J. Colloid Interface Sci.* **2018**, *519*, 273−284.
(31) Guillou, N.; Bourrelly, S.; Llewellyn, P. L.; Walton, R. I.; Millange, F. Location of CO_2 during its uptake by the flexible porous metal−organic framework MIL-53(Fe): a high resolution powder X-ray diffraction study. *CrystEngComm* **2015**, *17*, 422−429.
(32) Xiong, W.; Zeng, Z.; Li, X.; Zeng, G.; Xiao, R.; Yang, Z.; Zhou, Y.; Zhang, C.; Cheng, M.; Hu, L.; Zhou, C.; Qin, L.; Xu, R.; Zhang, Y. Multi-Walled Carbon Nanotube/Amino-Functionalized MIL-53(Fe) Composites: Remarkable Adsorptive Removal of Antibiotics from Aqueous Solutions. *Chemosphere* **2018**, *210*, 1061−1069.
(33) Millange, F.; Guillou, N.; Walton, R. I.; Grenèche, J.-M.; Margiolaki, I.; Férey, G. Effect of the Nature of the Metal on the Breathing Steps in MOFs with Dynamic Frameworks. *Chem. Commun.* **2008**, 4732−4734.
(34) Whitfield, T. R.; Wang, X.; Liu, L.; Jacobson, A. J. Metal-Organic Frameworks Based on Iron Oxide Octahedral Chains Connected by Benzenedicarboxylate Dianions. *Solid State Sci.* **2005**, *7*, 1096−1103.
(35) Medina, M. E.; Dumont, Y.; Grenèche, J.-M.; Millange, F.; et al. *Chem. Commun.* **2010**, *46*, 7987−7989.
(36) Wang, N.; Zhu, L.; Wang, D.; Wang, M.; Lin, Z.; Tang, H. Sono-Assisted Preparation of Highly-Efficient Peroxidase-Like Fe3O4 Magnetic Nanoparticles for Catalytic Removal of Organic Pollutants With H_2O_2. *Ultrason. Sonochem.* **2010**, *17*, 526−533.
(37) Lu, L.; Ai, Z.; Li, J.; Zheng, Z.; Li, Q.; Zhang, L. Synthesis and Characterization of Fe−Fe_2O_3 Core−Shell Nanowires and Nanonecklaces. *Cryst. Growth Des.* **2007**, *7*, 459−464.
(38) Araya, T.; Jia, M.; Yang, J.; Zhao, P.; Cai, K.; Ma, W.; Huang, Y. Resin Modified MIL-53 (Fe) MOF for Improvement of Photocatalytic Performance. *Appl. Catal., B* **2017**, *203*, 768−777.
(39) Wei, Y.-S.; Zhang, M.; Liao, P.-Q.; Lin, R.-B.; Li, T.-Y.; Shao, G.; Zhang, J.-P.; Chen, X.-M. Coordination Templated [2+2+2] Cyclotrimerization in a Porous Coordination Framework. *Nat. Commun.* **2015**, *6*, 8348.
(40) Lebedev, O. I.; Millange, F.; Serre, C.; Van Tendeloo, G.; Férey, G. First Direct Imaging of Giant Pores of the Metal−Organic Framework MIL-101. *Chem. Mater.* **2005**, *17*, 6525−6527.
(41) Loiseau, T.; Serre, C.; Huguenard, C.; Fink, G.; Taulelle, F.; Henry, M.; Bataille, T.; Férey, G. A Rationale for the Large Breathing of the Porous Aluminum Terephthalate (MIL-53) upon Hydration. *Chemistry* **2004**, *10*, 1373−1382.

DOI: 10.1021/acsami.9b05829
ACS Appl. Mater. Interfaces XXXX, XXX, XXX−XXX

(42) Alvaro, M.; Carbonell, E.; Ferrer, B.; Llabrés i Xamena, F. X.; Garcia, H. Semiconductor Behavior of a Metal-Organic Framework (MOF). *Chemistry* **2007**, *13*, 5106−5112.
(43) Yang, Z.; Xu, X.; Liang, X.; Lei, C.; Wei, Y.; He, P.; Lv, B.; Ma, H.; Lei, Z. MIL-53(Fe)-graphene Nanocomposites: Efficient Visible-Light Photocatalysts for the Selective Oxidation of Alcohols. *Appl. Catal., B* **2016**, *198*, 112−123.
(44) Fu, Y.; Sun, D.; Chen, Y.; Huang, R.; Ding, Z.; Fu, X.; Li, Z. An Amine-Functionalized Titanium Metal−Organic Framework Photocatalyst with Visible-Light-Induced Activity for CO_2 Reduction. *Angew. Chem. Int. Ed.* **2012**, *51*, 3364−3367.
(45) Cai, T.; Wang, L.; Liu, Y.; Zhang, S.; Dong, W.; Chen, H.; Yi, X.; Yuan, J.; Xia, X.; Liu, C.; Luo, S. Ag_3PO_4/Ti_3C_2 MXene Interface Materials as a Schottky Catalyst with Enhanced Photocatalytic Activities and Anti-Photocorrosion Performance. *Appl. Catal., B* **2018**, *239*, 545−554.
(46) Xu, D.; Cheng, B.; Cao, S.; Yu, J. Enhanced Photocatalytic Activity and Stability of Z-Scheme Ag 2 CrO 4 -GO Composite Photocatalysts for Organic Pollutant Degradation. *Appl. Catal., B* **2015**, *164*, 380−388.
(47) Meyer, K.; Ranocchiari, M.; van Bokhoven, J. A. Metal Organic Frameworks for Photo-Catalytic Water Splitting. *Energy Environ. Sci.* **2015**, *8*, 1923−1937.
(48) Cai, T.; Liu, Y.; Wang, L.; Zhang, S.; Zeng, Y.; Yuan, J.; Ma, J.; Dong, W.; Liu, C.; Luo, S. Silver Phosphate-Based Z-Scheme Photocatalytic System with Superior Sunlight Photocatalytic Activities and Anti-photocorrosion Performance. *Appl. Catal., B* **2017**, *208*, 1−13.
(49) Bai, S.; Jiang, J.; Zhang, Q.; Xiong, Y. Steering Charge Kinetics in Photocatalysis: Intersection of Materials Syntheses, Characterization Techniques and Theoretical Simulations. *Chem. Soc. Rev.* **2015**, *44*, 2893−2939.
(50) Chiu, Y.-H.; Hsu, Y.-J. Au@Cu 7 S 4 Yolk@Shell Nanocrystal-Decorated TiO_2 Nanowires as an All-day-active Photocatalyst for Environmental Purification. *Nano Energy* **2017**, *31*, 286−295.
(51) Ai, L.; Zhang, C.; Li, L.; Jiang, J. Iron Terephthalate Metal−Organic Framework: Revealing the Effective Activation of Hydrogen Peroxide for the Degradation of Organic Dye under Visible Light Irradiation. *Appl. Catal., B* **2014**, *148-149*, 191−200.
(52) Luo, J.; Liu, T.; Zhang, D.; Yin, K.; Wang, D.; Zhang, W.; Liu, C.; Yang, C.; Wei, Y.; Wang, L.; Luo, S.; Crittenden, J. C. The Individual and Co-exposure Degradation of Benzophenone Derivatives by UV/H2O2 and UV/PDS in Different Water Matrices. *Water Res.* **2019**, *159*, 102−110.
(53) Tang, J.; Wang, J. Metal Organic Framework with Coordinatively Unsaturated Sites as Efficient Fenton-like Catalyst for Enhanced Degradation of Sulfamethazine. *Environ. Sci. Technol.* **2018**, *52*, 5367−5377.

DOI: 10.1021/acsami.9b05829
ACS Appl. Mater. Interfaces XXXX, XXX, XXX−XXX